

Measurement of the W boson helicity in top quark decays using 5.4 fb⁻¹ of $p\bar{p}$ collision data

V.M. Abazov,³⁵ B. Abbott,⁷² B.S. Acharya,²⁹ M. Adams,⁴⁸ T. Adams,⁴⁶ G.D. Alexeev,³⁵ G. Alkhalaf,³⁹ A. Alton,^{a,60} G. Alverson,⁵⁹ G.A. Alves,² L.S. Ancu,³⁴ M. Aoki,⁴⁷ Y. Arnaud,¹⁴ M. Arov,⁵⁷ A. Askew,⁴⁶ B. Åsman,⁴⁰ O. Atramentov,⁶⁴ C. Avila,⁸ J. BackusMayes,⁷⁹ F. Badaud,¹³ L. Bagby,⁴⁷ B. Baldin,⁴⁷ D.V. Bandurin,⁴⁶ S. Banerjee,²⁹ E. Barberis,⁵⁹ P. Baringer,⁵⁵ J. Barreto,² J.F. Bartlett,⁴⁷ U. Bassler,¹⁸ V. Bazterra,⁴⁸ S. Beale,⁶ A. Bean,⁵⁵ M. Begalli,³ M. Begel,⁷⁰ C. Belanger-Champagne,⁴⁰ L. Bellantoni,⁴⁷ S.B. Beri,²⁷ G. Bernardi,¹⁷ R. Bernhard,²² I. Bertram,⁴¹ M. Besançon,¹⁸ R. Beuselinck,⁴² V.A. Bezzubov,³⁸ P.C. Bhat,⁴⁷ V. Bhatnagar,²⁷ G. Blazey,⁴⁹ S. Blessing,⁴⁶ K. Bloom,⁶³ A. Boehnlein,⁴⁷ D. Boline,⁶⁹ T.A. Bolton,⁵⁶ E.E. Boos,³⁷ G. Borissov,⁴¹ T. Bose,⁵⁸ A. Brandt,⁷⁵ O. Brandt,²³ R. Brock,⁶¹ G. Brooijmans,⁶⁷ A. Bross,⁴⁷ D. Brown,¹⁷ J. Brown,¹⁷ X.B. Bu,⁴⁷ M. Buehler,⁷⁸ V. Buescher,²⁴ V. Bunichev,³⁷ S. Burdin,^{b,41} T.H. Burnett,⁷⁹ C.P. Buszello,⁴⁰ B. Calpas,¹⁵ E. Camacho-Pérez,³² M.A. Carrasco-Lizarraga,⁵⁵ B.C.K. Casey,⁴⁷ H. Castilla-Valdez,³² S. Chakrabarti,⁶⁹ D. Chakraborty,⁴⁹ K.M. Chan,⁵³ A. Chandra,⁷⁷ G. Chen,⁵⁵ S. Chevalier-Théry,¹⁸ D.K. Cho,⁷⁴ S.W. Cho,³¹ S. Choi,³¹ B. Choudhary,²⁸ T. Christoudias,⁴² S. Cihangir,⁴⁷ D. Claes,⁶³ J. Clutter,⁵⁵ M. Cooke,⁴⁷ W.E. Cooper,⁴⁷ M. Corcoran,⁷⁷ F. Couderc,¹⁸ M.-C. Cousinou,¹⁵ A. Croc,¹⁸ D. Cutts,⁷⁴ M. Cwiok,³⁰ A. Das,⁴⁴ G. Davies,⁴² K. De,⁷⁵ S.J. de Jong,³⁴ E. De La Cruz-Burelo,³² F. Déliot,¹⁸ M. Demarteau,⁴⁷ R. Demina,⁶⁸ D. Denisov,⁴⁷ S.P. Denisov,³⁸ S. Desai,⁴⁷ K. DeVaughan,⁶³ H.T. Diehl,⁴⁷ M. Diesburg,⁴⁷ A. Dominguez,⁶³ T. Dorland,⁷⁹ A. Dubey,²⁸ L.V. Dudko,³⁷ D. Duggan,⁶⁴ A. Duperrin,¹⁵ S. Dutt,²⁷ A. Dyshkant,⁴⁹ M. Eads,⁶³ D. Edmunds,⁶¹ J. Ellison,⁴⁵ V.D. Elvira,⁴⁷ Y. Enari,¹⁷ H. Evans,⁵¹ A. Evdokimov,⁷⁰ V.N. Evdokimov,³⁸ G. Facini,⁵⁹ T. Ferbel,⁶⁸ F. Fiedler,²⁴ F. Filthaut,³⁴ W. Fisher,⁶¹ H.E. Fisk,⁴⁷ M. Fortner,⁴⁹ H. Fox,⁴¹ S. Fuess,⁴⁷ T. Gadfort,⁷⁰ A. Garcia-Bellido,⁶⁸ V. Gavrilov,³⁶ P. Gay,¹³ W. Geist,¹⁹ W. Geng,^{15,61} D. Gerbaudo,⁶⁵ C.E. Gerber,⁴⁸ Y. Gershtein,⁶⁴ G. Ginther,^{47,68} G. Golovanov,³⁵ A. Goussiou,⁷⁹ P.D. Grannis,⁶⁹ S. Greder,¹⁹ H. Greenlee,⁴⁷ Z.D. Greenwood,⁵⁷ E.M. Gregores,⁴ G. Grenier,²⁰ Ph. Gris,¹³ J.-F. Grivaz,¹⁶ A. Grohsjean,¹⁸ S. Grünendahl,⁴⁷ M.W. Grünewald,³⁰ F. Guo,⁶⁹ G. Gutierrez,⁴⁷ P. Gutierrez,⁷² A. Haas,^{c,67} S. Hagopian,⁴⁶ J. Haley,⁵⁹ L. Han,⁷ K. Harder,⁴³ A. Harel,⁶⁸ J.M. Hauptman,⁵⁴ J. Hays,⁴² T. Head,⁴³ T. Hebbeker,²¹ D. Hedin,⁴⁹ H. Hegab,⁷³ A.P. Heinson,⁴⁵ U. Heintz,⁷⁴ C. Hensel,²³ I. Heredia-De La Cruz,³² K. Herner,⁶⁰ G. Hesketh,⁵⁹ M.D. Hildreth,⁵³ R. Hirosky,⁷⁸ T. Hoang,⁴⁶ J.D. Hobbs,⁶⁹ B. Hoeneisen,¹² M. Hohlfeld,²⁴ S. Hossain,⁷² Z. Hubacek,^{10,18} N. Huske,¹⁷ V. Hynek,¹⁰ I. Iashvili,⁶⁶ R. Illingworth,⁴⁷ A.S. Ito,⁴⁷ S. Jabeen,⁷⁴ M. Jaffré,¹⁶ S. Jain,⁶⁶ D. Jamin,¹⁵ R. Jesik,⁴² K. Johns,⁴⁴ M. Johnson,⁴⁷ D. Johnston,⁶³ A. Jonckheere,⁴⁷ P. Jonsson,⁴² J. Joshi,²⁷ A. Juste,^{d,47} K. Kaadze,⁵⁶ E. Kajfasz,¹⁵ D. Karmanov,³⁷ P.A. Kasper,⁴⁷ I. Katsanos,⁶³ R. Kehoe,⁷⁶ S. Kermiche,¹⁵ N. Khalatyan,⁴⁷ A. Khanov,⁷³ A. Kharchilava,⁶⁶ Y.N. Kharzheev,³⁵ D. Khatidze,⁷⁴ M.H. Kirby,⁵⁰ J.M. Kohli,²⁷ A.V. Kozelov,³⁸ J. Kraus,⁶¹ A. Kumar,⁶⁶ A. Kupco,¹¹ T. Kurča,²⁰ V.A. Kuzmin,³⁷ J. Kvita,⁹ S. Lammers,⁵¹ G. Landsberg,⁷⁴ P. Lebrun,²⁰ H.S. Lee,³¹ S.W. Lee,⁵⁴ W.M. Lee,⁴⁷ J. Lellouch,¹⁷ L. Li,⁴⁵ Q.Z. Li,⁴⁷ S.M. Lietti,⁵ J.K. Lim,³¹ D. Lincoln,⁴⁷ J. Linnemann,⁶¹ V.V. Lipaev,³⁸ R. Lipton,⁴⁷ Y. Liu,⁷ Z. Liu,⁶ A. Lobodenko,³⁹ M. Lokajicek,¹¹ P. Love,⁴¹ H.J. Lubatti,⁷⁹ R. Luna-Garcia,^{e,32} A.L. Lyon,⁴⁷ A.K.A. Maciel,² D. Mackin,⁷⁷ R. Madar,¹⁸ R. Magaña-Villalba,³² S. Malik,⁶³ V.L. Malyshev,³⁵ Y. Maravin,⁵⁶ J. Martínez-Ortega,³² R. McCarthy,⁶⁹ C.L. McGivern,⁵⁵ M.M. Meijer,³⁴ A. Melnitchouk,⁶² D. Menezes,⁴⁹ P.G. Mercadante,⁴ M. Merkin,³⁷ A. Meyer,²¹ J. Meyer,²³ N.K. Mondal,²⁹ G.S. Muanza,¹⁵ M. Mulhearn,⁷⁸ E. Nagy,¹⁵ M. Naimuddin,²⁸ M. Narain,⁷⁴ R. Nayyar,²⁸ H.A. Neal,⁶⁰ J.P. Negret,⁸ P. Neustroev,³⁹ S.F. Novaes,⁵ T. Nunnemann,²⁵ G. Obrant,³⁹ J. Orduna,³² N. Osman,⁴² J. Osta,⁵³ G.J. Otero y Garzón,¹ M. Owen,⁴³ M. Padilla,⁴⁵ M. Pangilinan,⁷⁴ N. Parashar,⁵² V. Parihar,⁷⁴ S.K. Park,³¹ J. Parsons,⁶⁷ R. Partridge,^{c,74} N. Parua,⁵¹ A. Patwa,⁷⁰ B. Penning,⁴⁷ M. Perfilov,³⁷ K. Peters,⁴³ Y. Peters,⁴³ G. Petrillo,⁶⁸ P. Pétrouff,¹⁶ R. Piegaia,¹ J. Piper,⁶¹ M.-A. Pleier,⁷⁰ P.L.M. Podesta-Lerma,^{f,32} V.M. Podstavkov,⁴⁷ M.-E. Pol,² P. Polozov,³⁶ A.V. Popov,³⁸ M. Prewitt,⁷⁷ D. Price,⁵¹ S. Protopopescu,⁷⁰ J. Qian,⁶⁰ A. Quadt,²³ B. Quinn,⁶² M.S. Rangel,² K. Ranjan,²⁸ P.N. Ratoff,⁴¹ I. Razumov,³⁸ P. Renkel,⁷⁶ P. Rich,⁴³ M. Rijssenbeek,⁶⁹ I. Ripp-Baudot,¹⁹ F. Rizatdinova,⁷³ M. Rominsky,⁴⁷ C. Royon,¹⁸ P. Rubinov,⁴⁷ R. Ruchti,⁵³ G. Safronov,³⁶ G. Sajot,¹⁴ A. Sánchez-Hernández,³² M.P. Sanders,²⁵ B. Sanghi,⁴⁷ A.S. Santos,⁵ G. Savage,⁴⁷ L. Sawyer,⁵⁷ T. Scanlon,⁴² R.D. Schamberger,⁶⁹ Y. Scheglov,³⁹ H. Schellman,⁵⁰ T. Schliephake,²⁶ S. Schlobohm,⁷⁹ C. Schwanenberger,⁴³ R. Schwienhorst,⁶¹ J. Sekaric,⁵⁵ H. Severini,⁷² E. Shabalina,²³ V. Shary,¹⁸

A.A. Shchukin,³⁸ R.K. Shivpuri,²⁸ V. Simak,¹⁰ V. Sirotenko,⁴⁷ P. Skubic,⁷² P. Slattery,⁶⁸ D. Smirnov,⁵³
 K.J. Smith,⁶⁶ G.R. Snow,⁶³ J. Snow,⁷¹ S. Snyder,⁷⁰ S. Söldner-Rembold,⁴³ L. Sonnenschein,²¹ A. Sopczak,⁴¹
 M. Sosebee,⁷⁵ K. Soustruznik,⁹ B. Spurlock,⁷⁵ J. Stark,¹⁴ V. Stolin,³⁶ D.A. Stoyanova,³⁸ M. Strauss,⁷² D. Strom,⁴⁸
 L. Stutte,⁴⁷ L. Suter,⁴³ P. Svoisky,⁷² M. Takahashi,⁴³ A. Tanasijczuk,¹ W. Taylor,⁶ M. Titov,¹⁸ V.V. Tokmenin,³⁵
 Y.-T. Tsai,⁶⁸ D. Tsybychev,⁶⁹ B. Tuchming,¹⁸ C. Tully,⁶⁵ P.M. Tuts,⁶⁷ L. Uvarov,³⁹ S. Uvarov,³⁹ S. Uzunyan,⁴⁹
 R. Van Kooten,⁵¹ W.M. van Leeuwen,³³ N. Varelas,⁴⁸ E.W. Varnes,⁴⁴ I.A. Vasilyev,³⁸ P. Verdier,²⁰
 L.S. Vertogradov,³⁵ M. Verzocchi,⁴⁷ M. Vesterinen,⁴³ D. Vilanova,¹⁸ P. Vint,⁴² P. Vokac,¹⁰ H.D. Wahl,⁴⁶
 M.H.L.S. Wang,⁶⁸ J. Warchol,⁵³ G. Watts,⁷⁹ M. Wayne,⁵³ M. Weber,^{9,47} L. Welty-Rieger,⁵⁰ A. White,⁷⁵ D. Wicke,²⁶
 M.R.J. Williams,⁴¹ G.W. Wilson,⁵⁵ S.J. Wimpenny,⁴⁵ M. Wobisch,⁵⁷ D.R. Wood,⁵⁹ T.R. Wyatt,⁴³ Y. Xie,⁴⁷
 C. Xu,⁶⁰ S. Yacoub,⁵⁰ R. Yamada,⁴⁷ W.-C. Yang,⁴³ T. Yasuda,⁴⁷ Y.A. Yatsunenkov,³⁵ Z. Ye,⁴⁷ H. Yin,⁴⁷ K. Yip,⁷⁰
 S.W. Youn,⁴⁷ J. Yu,⁷⁵ S. Zelitch,⁷⁸ T. Zhao,⁷⁹ B. Zhou,⁶⁰ J. Zhu,⁶⁰ M. Zielinski,⁶⁸ D. Zieminska,⁵¹ and L. Zivkovic⁶⁷

(The D0 Collaboration*)

- ¹Universidad de Buenos Aires, Buenos Aires, Argentina
²LAFEX, Centro Brasileiro de Pesquisas Físicas, Rio de Janeiro, Brazil
³Universidade do Estado do Rio de Janeiro, Rio de Janeiro, Brazil
⁴Universidade Federal do ABC, Santo André, Brazil
⁵Instituto de Física Teórica, Universidade Estadual Paulista, São Paulo, Brazil
⁶Simon Fraser University, Vancouver, British Columbia, and York University, Toronto, Ontario, Canada
⁷University of Science and Technology of China, Hefei, People's Republic of China
⁸Universidad de los Andes, Bogotá, Colombia
⁹Charles University, Faculty of Mathematics and Physics,
 Center for Particle Physics, Prague, Czech Republic
¹⁰Czech Technical University in Prague, Prague, Czech Republic
¹¹Center for Particle Physics, Institute of Physics,
 Academy of Sciences of the Czech Republic, Prague, Czech Republic
¹²Universidad San Francisco de Quito, Quito, Ecuador
¹³LPC, Université Blaise Pascal, CNRS/IN2P3, Clermont, France
¹⁴LPSC, Université Joseph Fourier Grenoble 1, CNRS/IN2P3,
 Institut National Polytechnique de Grenoble, Grenoble, France
¹⁵CPPM, Aix-Marseille Université, CNRS/IN2P3, Marseille, France
¹⁶LAL, Université Paris-Sud, CNRS/IN2P3, Orsay, France
¹⁷LPNHE, Universités Paris VI and VII, CNRS/IN2P3, Paris, France
¹⁸CEA, Irfu, SPP, Saclay, France
¹⁹IPHC, Université de Strasbourg, CNRS/IN2P3, Strasbourg, France
²⁰IPNL, Université Lyon 1, CNRS/IN2P3, Villeurbanne, France and Université de Lyon, Lyon, France
²¹III. Physikalisches Institut A, RWTH Aachen University, Aachen, Germany
²²Physikalisches Institut, Universität Freiburg, Freiburg, Germany
²³II. Physikalisches Institut, Georg-August-Universität Göttingen, Göttingen, Germany
²⁴Institut für Physik, Universität Mainz, Mainz, Germany
²⁵Ludwig-Maximilians-Universität München, München, Germany
²⁶Fachbereich Physik, Bergische Universität Wuppertal, Wuppertal, Germany
²⁷Panjab University, Chandigarh, India
²⁸Delhi University, Delhi, India
²⁹Tata Institute of Fundamental Research, Mumbai, India
³⁰University College Dublin, Dublin, Ireland
³¹Korea Detector Laboratory, Korea University, Seoul, Korea
³²CINVESTAV, Mexico City, Mexico
³³FOM-Institute NIKHEF and University of Amsterdam/NIKHEF, Amsterdam, The Netherlands
³⁴Radboud University Nijmegen/NIKHEF, Nijmegen, The Netherlands
³⁵Joint Institute for Nuclear Research, Dubna, Russia
³⁶Institute for Theoretical and Experimental Physics, Moscow, Russia
³⁷Moscow State University, Moscow, Russia
³⁸Institute for High Energy Physics, Protvino, Russia
³⁹Petersburg Nuclear Physics Institute, St. Petersburg, Russia
⁴⁰Stockholm University, Stockholm and Uppsala University, Uppsala, Sweden
⁴¹Lancaster University, Lancaster LA1 4YB, United Kingdom
⁴²Imperial College London, London SW7 2AZ, United Kingdom
⁴³The University of Manchester, Manchester M13 9PL, United Kingdom
⁴⁴University of Arizona, Tucson, Arizona 85721, USA
⁴⁵University of California Riverside, Riverside, California 92521, USA

- ⁴⁶Florida State University, Tallahassee, Florida 32306, USA
⁴⁷Fermi National Accelerator Laboratory, Batavia, Illinois 60510, USA
⁴⁸University of Illinois at Chicago, Chicago, Illinois 60607, USA
⁴⁹Northern Illinois University, DeKalb, Illinois 60115, USA
⁵⁰Northwestern University, Evanston, Illinois 60208, USA
⁵¹Indiana University, Bloomington, Indiana 47405, USA
⁵²Purdue University Calumet, Hammond, Indiana 46323, USA
⁵³University of Notre Dame, Notre Dame, Indiana 46556, USA
⁵⁴Iowa State University, Ames, Iowa 50011, USA
⁵⁵University of Kansas, Lawrence, Kansas 66045, USA
⁵⁶Kansas State University, Manhattan, Kansas 66506, USA
⁵⁷Louisiana Tech University, Ruston, Louisiana 71272, USA
⁵⁸Boston University, Boston, Massachusetts 02215, USA
⁵⁹Northeastern University, Boston, Massachusetts 02115, USA
⁶⁰University of Michigan, Ann Arbor, Michigan 48109, USA
⁶¹Michigan State University, East Lansing, Michigan 48824, USA
⁶²University of Mississippi, University, Mississippi 38677, USA
⁶³University of Nebraska, Lincoln, Nebraska 68588, USA
⁶⁴Rutgers University, Piscataway, New Jersey 08855, USA
⁶⁵Princeton University, Princeton, New Jersey 08544, USA
⁶⁶State University of New York, Buffalo, New York 14260, USA
⁶⁷Columbia University, New York, New York 10027, USA
⁶⁸University of Rochester, Rochester, New York 14627, USA
⁶⁹State University of New York, Stony Brook, New York 11794, USA
⁷⁰Brookhaven National Laboratory, Upton, New York 11973, USA
⁷¹Langston University, Langston, Oklahoma 73050, USA
⁷²University of Oklahoma, Norman, Oklahoma 73019, USA
⁷³Oklahoma State University, Stillwater, Oklahoma 74078, USA
⁷⁴Brown University, Providence, Rhode Island 02912, USA
⁷⁵University of Texas, Arlington, Texas 76019, USA
⁷⁶Southern Methodist University, Dallas, Texas 75275, USA
⁷⁷Rice University, Houston, Texas 77005, USA
⁷⁸University of Virginia, Charlottesville, Virginia 22901, USA
⁷⁹University of Washington, Seattle, Washington 98195, USA

(Dated: November 28, 2010)

We present a measurement of the helicity of the W boson produced in top quark decays using $t\bar{t}$ decays in the $\ell+$ jets and dilepton final states selected from a sample of 5.4 fb^{-1} of collisions recorded using the D0 detector at the Fermilab Tevatron $p\bar{p}$ collider. We measure the fractions of longitudinal and right-handed W bosons to be $f_0 = 0.669 \pm 0.102 [\pm 0.078 \text{ (stat.)} \pm 0.065 \text{ (syst.)}]$ and $f_+ = 0.023 \pm 0.053 [\pm 0.041 \text{ (stat.)} \pm 0.034 \text{ (syst.)}]$, respectively. This result is consistent at the 98% level with the standard model. A measurement with f_0 fixed to the value from the standard model yields $f_+ = 0.010 \pm 0.037 [\pm 0.022 \text{ (stat.)} \pm 0.030 \text{ (syst.)}]$.

PACS numbers: 14.65.Ha, 14.70.Fm, 12.15.Ji, 12.38.Qk, 13.38.Be, 13.88.+e

INTRODUCTION

The top quark is the heaviest known fundamental particle and was discovered in 1995 [1, 2] at the Tevatron proton-antiproton collider at Fermilab. The dominant top quark production mode at the Tevatron is $p\bar{p} \rightarrow t\bar{t}X$. Since the time of discovery, over 100 times more inte-

grated luminosity has been collected, providing a large number of $t\bar{t}$ events with which to study the properties of the top quark. In the standard model (SM), the branching ratio for the top quark to decay to a W boson and a b quark is $> 99.8\%$. The on-shell W boson from the top quark decay has three possible helicity states, and we define the fraction of W bosons produced in these states as f_0 (longitudinal), f_- (left-handed), and f_+ (right-handed). In the SM, the top quark decays via the $V - A$ charged weak current interaction, which strongly suppresses right-handed W bosons and predicts f_0 and f_- at leading order in terms of the top quark mass (m_t), W

*with visitors from ^aAugustana College, Sioux Falls, SD, USA, ^bThe University of Liverpool, Liverpool, UK, ^cSLAC, Menlo Park, CA, USA, ^dICREA/IFAE, Barcelona, Spain, ^eCentro de Investigacion en Computacion - IPN, Mexico City, Mexico, ^fECFM, Universidad Autonoma de Sinaloa, Culiacán, Mexico, and ^gUniversität Bern, Bern, Switzerland.

TABLE I: Summary of the most recent W boson helicity measurements from the D0 [6] and CDF [7] collaborations. The first uncertainty is statistical and the second systematic.

D0, 1 fb ⁻¹ [6]	$f_0 = 0.425 \pm 0.166 \pm 0.102,$
	$f_+ = 0.119 \pm 0.090 \pm 0.053$
	f_+ fixed: $f_0 = 0.619 \pm 0.090 \pm 0.052$
	f_0 fixed: $f_+ = -0.002 \pm 0.047 \pm 0.047$
CDF, 2.7 fb ⁻¹ [7]	$f_0 = 0.88 \pm 0.11 \pm 0.06,$
	$f_+ = -0.15 \pm 0.07 \pm 0.06$
	f_+ fixed: $f_0 = 0.70 \pm 0.07 \pm 0.04$
	f_0 fixed: $f_+ = -0.01 \pm 0.02 \pm 0.05$

boson mass (M_W), and b quark mass (m_b) to be [3]

$$f_0 = \frac{(1 - y^2)^2 - x^2(1 + y^2)}{(1 - y^2)^2 + x^2(1 - 2x^2 + y^2)} \quad (1)$$

$$f_- = \frac{x^2(1 - x^2 + y^2 + \sqrt{\lambda})}{(1 - y^2)^2 + x^2(1 - 2x^2 + y^2)} \quad (2)$$

$$f_+ = \frac{x^2(1 - x^2 + y^2 - \sqrt{\lambda})}{(1 - y^2)^2 + x^2(1 - 2x^2 + y^2)} \quad (3)$$

where $x = M_W/m_t$, $y = m_b/m_t$, and $\lambda = 1 + x^4 + y^4 - 2x^2y^2 - 2x^2 - 2y^2$. With the present measurements of $m_t = 173.3 \pm 1.1$ GeV/ c^2 [4] and $M_W = 80.399 \pm 0.023$ GeV/ c^2 [5], and taking m_b to be 5 GeV/ c^2 , the SM expected values are $f_0=0.698$, $f_- = 0.301$, and $f_+ = 4.1 \times 10^{-4}$. The absolute uncertainties on the SM expectations, which arise from uncertainties on the particle masses as well as contributions from higher-order effects, are $\approx (0.01 - 0.02)$ for f_0 and f_- , and $\mathcal{O}(10^{-3})$ for f_+ [3].

In this paper, we present a measurement of the W boson helicity fractions f_0 and f_+ and constrain the fraction f_- through the unitarity requirement of $f_- + f_+ + f_0 = 1$. Any significant deviation from the SM expectation would be an indication of new physics, arising from either a deviation from the expected $V - A$ coupling of the tWb vertex or the presence of non-SM events in the data sample. The most recently published results are summarized in Table I.

The extraction of the W boson helicities is based on the measurement of the angle θ^* between the opposite of the direction of the top quark and the direction of the down-type fermion (charged lepton or d , s quark) decay product of the W boson in the W boson rest frame. The dependence of the distribution of $\cos\theta^*$ on the W boson helicity fractions is given by

$$\omega(c) \propto 2(1 - c^2)f_0 + (1 - c)^2f_- + (1 + c)^2f_+ \quad (4)$$

with $c = \cos\theta^*$. After selection of a $t\bar{t}$ enriched sample the four-momenta of the $t\bar{t}$ decay products in each event are reconstructed as described below, permitting the calculation of $\cos\theta^*$. Once the $\cos\theta^*$ distribution is measured, the values of f_0 and f_+ are extracted with

a binned Poisson likelihood fit to the data. The measurement presented here is based on $p\bar{p}$ collisions at a center-of-mass energy $\sqrt{s} = 1.96$ TeV corresponding to an integrated luminosity of 5.4 fb⁻¹, five times more than the amount used in the result in Ref. [6].

DETECTOR

The D0 Run II detector [8] is a multipurpose detector which consists of three primary systems: a central tracking system, calorimeters, and a muon spectrometer. We use a standard right-handed coordinate system. The nominal collision point is the center of the detector with coordinate (0,0,0). The direction of the proton beam is the positive $+z$ axis. The $+x$ axis is horizontal, pointing away from the center of the Tevatron ring. The $+y$ axis points vertically upwards. The polar angle, θ , is defined such that $\theta = 0$ is the $+z$ direction. Usually, the polar angle is replaced by the pseudorapidity $\eta = -\ln \tan(\frac{\theta}{2})$. The azimuthal angle, ϕ , is defined such that $\phi = 0$ points along the $+x$ axis, away from the center of the Tevatron ring.

The silicon microstrip tracker (SMT) is the innermost part of the tracking system and has a six-barrel longitudinal structure, where each barrel consists of a set of four layers arranged axially around the beam pipe. A fifth layer of SMT sensors was installed near the beam pipe in 2006 [9]. The data set recorded before this addition is referred to as the ‘‘Run IIa’’ sample, and the subsequent data set is referred to as the ‘‘Run IIb’’ sample. Radial disks are interspersed between the barrel segments. The SMT provides a spatial resolution of approximately 10 μm in $r - \phi$ and 100 μm in $r - z$ (where r is the radial distance in the $x-y$ plane) and covers $|\eta| < 3$. The central fiber tracker (CFT) surrounds the SMT and consists of eight concentric carbon fiber barrels holding doublet layers of scintillating fibers (one axial and one small-angle stereo layer), with the outermost barrel covering $|\eta| < 1.7$. The solenoid surrounds the CFT and provides a 2 T uniform axial magnetic field.

The liquid-argon/uranium calorimeter system is housed in three cryostats, with the central calorimeter (CC) covering $|\eta| < 1.1$ and two end calorimeters (EC) covering $1.5 < |\eta| < 4.2$. The calorimeter is made up of unit cells consisting of an absorber plate and a signal board; liquid argon, the active material of the calorimeter, fills the gap. The inner part of the calorimeter is the electromagnetic (EM) section and the outer part is the hadronic section. The muon system is the outermost part of the D0 detector and covers $|\eta| < 2$. It is primarily made of two types of detectors, drift tubes and scintillators, and consists of three layers (A,B and C). Between layer A and layer B, there is magnetized steel with a 1.8 T toroidal field.

DATA AND SIMULATION SAMPLES

At the Tevatron, with proton and anti-proton bunches colliding at intervals of 396 ns, the collision rate is about 2.5 MHz. Out of these 2.5×10^6 beam crossings per second at D0, only those that produce events which are identified by a three-level trigger system as having properties matching the characteristics of physics events of interest are retained, at a rate of ~ 100 Hz [8, 10]. This analysis is performed using events collected with the triggers applicable for ℓ +jets and dilepton final states between April 2002 and June 2009, corresponding to a total integrated luminosity of 5.4 fb^{-1} . Analysis of the Run IIa sample, which totals about 1 fb^{-1} , was presented in Ref. [6]. Here we describe the analysis of the Run IIb data sample and then combine our result with the result from Ref. [6] when reporting our measurement from the full data sample.

The Monte Carlo (MC) simulated samples used for modeling the data are generated with ALPGEN [11] interfaced to PYTHIA [12] for parton shower simulation, passed through a detailed detector simulation based on GEANT [13], overlaid with data collected from a random subsample of beam crossings to model the effects of noise and multiple interactions, and reconstructed using the same algorithms that are used for data. For the signal ($t\bar{t}$) sample, we must model the distribution of $\cos\theta^*$ corresponding to any set of values for the W boson helicity fractions, a task that is complicated by the fact that ALPGEN can only produce linear combinations of $V - A$ and $V + A$ tWb couplings. Hence, for this analysis, we use samples that are either purely $V - A$ or purely $V + A$, and use a reweighting procedure (described below) to form models of arbitrary helicity states. ALPGEN is also used for generating all V +jets processes where V represents the vector bosons. PYTHIA is used for generating diboson (WW , WZ , and ZZ) backgrounds in the dilepton channels. Background from multijet production is modeled using data.

EVENT SELECTION

We expect *a priori* that our measurement will be limited by statistics, so our analysis strategy aims to maximize the acceptance for $t\bar{t}$ events. The selection is done in two steps. In the first step, a loose initial selection using data quality, trigger, object identification, and kinematic criteria is applied to define a sample with the characteristics of $t\bar{t}$ events. Subsequently, a multivariate likelihood discriminant is defined to separate the $t\bar{t}$ signal from the background in the data. We use events in the ℓ +jets and dilepton $t\bar{t}$ decay channels, which are defined below.

In the ℓ +jets decay $t\bar{t} \rightarrow W^+ W^- b\bar{b} \rightarrow \ell\nu qq'\bar{b}\bar{b}$, events contain one charged lepton (where lepton here refers to an electron or a muon), at least four jets with two of them being b quark jets, and significant miss-

ing transverse energy \cancel{E}_T (defined as the opposite of the vector sum of the transverse energies in each calorimeter cell, corrected for the energy carried by identified muons and energy added or subtracted due to the jet energy calibration described below). The event selection requires at least four jets with transverse momentum $p_T > 20 \text{ GeV}/c$ and $|\eta| < 2.5$ with the leading jet $p_T > 40 \text{ GeV}/c$. At least one lepton is required with $p_T > 20 \text{ GeV}/c$ and $|\eta| < 1.1$ (2.0) for electrons (muons). Requirements are also made on the value of \cancel{E}_T and the angle between the \cancel{E}_T vector and the lepton (to reduce the contribution of events in which mis-measurement of the lepton energy gives rise the spurious \cancel{E}_T): in the e +jets channel the requirement is $\cancel{E}_T > 20 \text{ GeV}$ and $\Delta\phi(e, \cancel{E}_T) > 0.7\pi - 0.045 \cdot \cancel{E}_T/\text{GeV}$, and in the μ +jets channel the requirement is $\cancel{E}_T > 25 \text{ GeV}$ and $\Delta\phi(\mu, \cancel{E}_T) > 2.1 - 0.035 \cdot \cancel{E}_T/\text{GeV}$. In addition, for the μ +jets channel, the invariant mass of the selected muon and any other muon in the event is required to be outside of the Z boson mass window ($< 70 \text{ GeV}/c^2$ or $> 100 \text{ GeV}/c^2$).

For the dilepton decay channel, $t\bar{t} \rightarrow W^+ W^- b\bar{b} \rightarrow \bar{\ell}\nu\ell'\nu'b\bar{b}$, the signature is two leptons of opposite charge, two b quark jets, and significant \cancel{E}_T . The event selection requires at least two jets with $p_T > 20 \text{ GeV}/c$ and $|\eta| < 2.5$ and two leptons (electron or muon) with $p_T > 20 \text{ GeV}/c$. The muons are required to have $|\eta| < 2.0$, and the electrons are required to have $|\eta| < 1.1$ or $1.5 < |\eta| < 2.5$.

Jets are defined using a mid-point cone algorithm [14] with radius 0.5. Their energies are first calibrated to be equal, on average, to the sums of the energies of the particles within the jet cone. This calibration accounts for the energy response of the calorimeters, the energy that crosses the cone boundary due to the transverse shower size, and the additional energy from event pileup and multiple $p\bar{p}$ interactions in a single beam crossing. The energy added to or subtracted from each jet in due to the above calibration is propagated to the calculation of \cancel{E}_T . Subsequently, an additional correction to for the average energy radiated by gluons outside of the jet cone is applied to the jet energy. Electrons are identified by their energy deposition and shower shape in the calorimeter combined with information from the tracking system. Muons are identified using information from the muon detector and the tracking system. We require the (two) highest- p_T lepton(s) to be isolated from other tracks and calorimeter energy deposits in the ℓ +jets (dilepton) channel. For all channels, we require a well-reconstructed $p\bar{p}$ vertex (PV) with the distance in z between this vertex and the point of closest approach of the lepton track being less than 1 cm.

The main sources of background after the initial selection in the ℓ +jets channel are W +jets and multijet production; in the dilepton channels they are Z boson and diboson production as well as multijet and W +jets pro-

duction. Events with fewer leptons than required (multijet events, or W +jets events in the dilepton channel) can enter the sample when jets are either misidentified as leptons or contain a lepton from semileptonic quark decay that passes the electron likelihood or muon isolation criterion. In all cases they are modeled using data with relaxed lepton identification or isolation criteria. The multijet contribution to the ℓ +jets final states in the initially-selected sample is estimated from data following the method described in Ref. [16]. This method relies on the selection of two data samples, one (the tight sample) with the standard lepton criteria, and the other (the loose sample) with relaxed isolation or identification criteria. The numbers of events in each sample are:

$$N_{\text{loose}} = N^{t\bar{t}+W} + N^{\text{MJ}} \quad (5)$$

$$N_{\text{tight}} = \varepsilon_{\ell} N^{t\bar{t}+W} + \varepsilon_{\text{MJ}} N^{\text{MJ}} \quad (6)$$

Here the coefficient ε_{ℓ} is the efficiency for isolated leptons in $t\bar{t}$ or $Wjjjj$ events to satisfy the standard lepton requirements, while ε_{MJ} is the efficiency for a jet in multijet events to satisfy those requirements. We measure ε_{ℓ} in $Z \rightarrow \ell\ell$ control samples and ε_{MJ} in multijet control samples. Inserting the measured values, we solve Eqs. 5 and 6 to obtain the number of multijet events (N^{MJ}) and the number of events with isolated leptons ($N^{t\bar{t}+W}$). In the dilepton channels we model the background due to jets being misidentified as isolated leptons using data events where both leptons have the same charge. This background originates from multijets events with two jets misidentified as leptons and from W +jets events with one jet misidentified as a lepton.

To separate the $t\bar{t}$ signal from these sources of background, we define a multivariate likelihood and retain only events above a certain threshold in the value of that likelihood. The set of variables used in the likelihood and the threshold value are optimized separately for each $t\bar{t}$ decay channel. The first step in the optimization procedure is to identify a set of candidate variables that may be used in the likelihood. The set we consider is:

- **Aplanarity \mathcal{A}** , defined as 3/2 of the smallest eigenvalue of the normalized momentum tensor for the jets (in the ℓ +jets channels) or jets and leptons (in the dilepton channels). The aplanarity \mathcal{A} is a measure of the deviation from flatness of the event, and $t\bar{t}$ events tend to have larger values than background.
- **Sphericity \mathcal{S}** , defined as 3/2 of the sum of the two smallest eigenvalues of the normalized momentum tensor for the jets (in the ℓ +jets channels) or jets and leptons (in the dilepton channels). This variable is a measure of the isotropy of the energy

flow in the event, and $t\bar{t}$ events tend to have larger values than background.

- **H_T** , introduced in Refs. [17] and [18], is defined as the scalar sum of the jets' p_T values. Jets arising from gluon radiation often have lower p_T than jets in $t\bar{t}$ events, so background events tend to have smaller values of H_T than signal.
- **Centrality \mathcal{C}** , defined as $\frac{H_T}{H_E}$ where H_E is the sum of all jet energies. The centrality \mathcal{C} is similar to H_T but normalized in a way to minimize dependence on the top quark mass.
- **$K'_{T\text{min}}$** , defined as $\Delta R_{jj\text{min}} \cdot \frac{E_{T\text{min}}}{E_T^W}$, where $\Delta R_{jj\text{min}}$ is the distance in $\eta - \phi$ space between the closest pair of jets, $E_{T\text{min}}$ is the lowest jet E_T value in the pair, and E_T^W is the transverse energy of the leptonically-decaying W boson (in the dilepton channels E_T^W is the magnitude of the vector sum of the \cancel{E}_T and leading lepton p_T). Only the four leading- E_T jets are considered in computing this variable. Jets arising from gluon radiation (as is the case for most of the background) tend to have lower values of $K'_{T\text{min}}$.
- **$m_{jj\text{min}}$** , defined as the smallest dijet mass of pairs of selected jets. This variable is sensitive to gluon radiation and tends to be smaller for background than signal.
- **h** , defined as the scalar sum of all the selected jet and lepton energies. Jets arising from gluon radiation often have lower energy than jets in $t\bar{t}$ events, and leptons arising from the decay of heavy flavor jets often have lower energy than leptons from W boson decay, so background events tend to have smaller values of h than signal.
- **χ_k^2** , defined as the χ^2 for a kinematic fit of ℓ +jets final states to the $t\bar{t}$ hypothesis. Signal events tend to have smaller χ^2 values than background. This variable is not used for dilepton events, for which a kinematic fit is underconstrained.
- **$\Delta\phi(\text{lepton}, \cancel{E}_T)$** , defined as the angle between the leading lepton and the \cancel{E}_T . W +jets events with \cancel{E}_T arising from mismeasured lepton p_T tend to have $\Delta\phi(\text{lepton}, \cancel{E}_T) \approx 0$ or π .
- **b jet content of the event**. Due to the long lifetime of the b quark, tracks within jets arising from b quarks have different properties (such as larger impact parameters with respect to the PV and the presence of secondary decay vertices) than tracks within light-quark or gluon jets. The consistency of a given jet with the hypothesis that the jet was produced by a b quark is quantified with a neural

network (NN) that considers several properties of the tracks contained within the jet cone [15]. In the ℓ +jets channels, we take the average of the NN values NN_b of the two most b -like jets to form a variable called $NN_{b\text{avg}}$, and in the dilepton channels we take the NN_b values of the two most b -like jets as separate variables NN_{b1} (the largest NN_b value) and NN_{b2} (the second-largest NN_b value). For top quark events, these variables tend to be close to one, while for events containing only light jets they tend to be close to zero.

- \cancel{E}_T or χ_Z^2 . For the $e\mu$ and ee channels only, \cancel{E}_T is considered as a variable in the likelihood discriminant. In the $\mu\mu$ channel, where spurious \cancel{E}_T can arise from mismeasurement of the muon momentum, we instead use χ_Z^2 , the χ^2 of a kinematic fit to the $Z \rightarrow \mu\mu$ hypothesis.
- **Dilepton mass $m_{\ell\ell}$** . Also for the dilepton channels only, the invariant mass of the lepton pairs is considered as a variable in the classical likelihood. The motivation is to discriminate against Z boson production.

We consider all combinations of the above variables to select the optimal set to use for each $t\bar{t}$ decay channel. For a given combination of variables, the likelihood ratio L_t is defined as

$$L_t = \frac{\exp\left\{\sum_{i=1}^{N_{\text{var}}}\left[\ln\left(\frac{S}{B}\right)_i^{\text{fit}}\right]\right\}}{\exp\left\{\sum_{i=1}^{N_{\text{var}}}\left[\ln\left(\frac{S}{B}\right)_i^{\text{fit}}\right]\right\} + 1}, \quad (7)$$

where N_{var} is the number of input variables used in the likelihood, and $(\frac{S}{B})_i^{\text{fit}}$ is the ratio of the parameterized signal and background probability density functions. We consider all possible subsets of the above variables to be used in L_t and scan across all potential selection criteria on L_t . For each L_t definition and prospective selection criterion, we compute the following figure of merit (FOM):

$$\text{FOM} = \frac{N_S}{\sqrt{N_S + N_B + \sigma_B^2}}, \quad (8)$$

where N_S and N_B are the numbers of signal and background events expected to satisfy the L_t selection.

The term σ_B reflects the uncertainty in the background selection efficiency arising from any mis-modeling of the input variables in the MC. To assess σ_B , we compare each variable in data and MC in background-dominated samples. The background-dominated samples are created by forming a multivariate likelihood ratio (Eq. 7) that does not use the variable under study, nor any variable that is

strongly correlated with it, where the criterion is a correlation coefficient between -0.10 and 0.10 . We select events that have low values of this likelihood, and are therefore unlikely to be $t\bar{t}$ events, such that 95% of MC $t\bar{t}$ events are rejected. Because the $t\bar{t}$ contribution to the selected data sample is negligible, we can directly compare the background model to data. The impact of any mis-modeling on the likelihood distribution is assessed by taking the ratio of the observed to the expected distributions as a function of each variable and fitting this to a polynomial. The result is that for each variable i we build a function k_i that encodes the data/MC discrepancies in that variable. For each simulated background event, we reweight each likelihood according to the data/MC differences. For example, for a likelihood that uses n of the possible variables, the likelihood is given a weight

$$w = \prod_{i=1}^n k_i(v_i). \quad (9)$$

The quantity σ_B is the difference in the predicted background yield when the unweighted and weighted L_t distributions are used for background. This uncertainty is propagated through the analysis as one component of the total uncertainty in the background yield.

TABLE II: The set of variables chosen for use in L_t for the e +jets and μ +jets channels. The numbers of background and $t\bar{t}$ events in the initially-selected data, as determined from a fit to the L_t distribution, are also presented.

	e +jets	μ +jets
Events passing initial selection	1442	1250
Variables in best L_t	\mathcal{C}	\mathcal{C}
	H_T	H_T
	$K'_{T\text{min}}$	$K'_{T\text{min}}$
	$NN_{b\text{avg}}$	$NN_{b\text{avg}}$
	χ_k^2	h
	$m_{jj\text{min}}$	
	Aplanarity	
$N(t\bar{t})$	592.6 ± 31.8	612.7 ± 31.0
$N(W+\text{jets})$	690.2 ± 21.8	579.8 ± 18.6
$N(\text{multijet})$	180.3 ± 9.9	6.5 ± 4.9

The sets of variables and L_t selection criteria that maximize the FOM defined in Eq. 8 for each $t\bar{t}$ final state are shown in Tables II and III. Figures 1-5 show the distributions of the variables in the best likelihood discriminant L_t for the events passing the preselection cuts, where the signal and background contributions are normalized as described below. In addition, we use L_t to determine the signal and background content of the initially-selected sample by performing a binned Poisson maximum likelihood fit to the L_t distribution where the signal and total background normalizations are free parameters. The W +jets contribution is determined by the fit to the L_t distribution, while the multijet component is constrained to be consistent with the value determined from Eqs. 5

TABLE III: The set of variables chosen for use in L_t for the dilepton channels. The number of background and $t\bar{t}$ events in the initially-selected data, as determined from a fit to the L_t distribution, are also presented.

	$e\mu$	ee	$\mu\mu$
Events passing initial selection	323	3275	5740
Variables in optimized L_t	$\mathcal{A}, \mathcal{S}, h, m_{jj\min}$ $K'_{T\min}, \cancel{E}_T, \text{NN}_{b1}, m_{\ell\ell}$	$\mathcal{A}, \mathcal{S}, m_{jj\min}$ $\cancel{E}_T, \text{NN}_{b1}, m_{\ell\ell}$	$\mathcal{A}, \mathcal{S}, m_{jj\min}, K'_{T\min}$ χ^2_k, NN_{b1}
$N(t\bar{t})$	178.7 ± 15.6	74.9 ± 10.7	86.0 ± 13.8
$N(\text{background})$	144.3 ± 14.5	3200 ± 57	5654 ± 76

and 6. In the dilepton channels the relative contributions of the different background sources are fixed according to their expected yield, but the total background is allowed to float. The signal and background yields in the initially-selected sample for the ℓ +jets channels are listed in Table II, and for the dilepton channels in Table III. Figures 6 and 7 show the distribution of the best likelihood discriminant for each channel, where the signal and background contributions are normalized according to the values returned by the fit. Tables IV and V show the optimal L_t cut value for each channel and the final number of events in data and the expected numbers of signal and background events after applying the L_t requirement.

TABLE IV: Expected background and $t\bar{t}$ yields, and the number of events observed, after the selection on L_t in the ℓ +jets decay channels.

	e +jets	μ +jets
Optimized L_t requirement	> 0.58	> 0.29
$t\bar{t}$	484.4 ± 41.4	567.2 ± 47.3
W +jets	111.7 ± 12.6	227.7 ± 19.2
Multijet	58.1 ± 3.9	4.0 ± 3.1
Total	656.2 ± 43.4	798.9 ± 51.2
Observed	628	803

TABLE V: Expected background and $t\bar{t}$ yields, and the number of events observed, after the selection on L_t in the dilepton decay channels.

Source	$e\mu$	ee	$\mu\mu$
Optimized L_t requirement	> 0.28	> 0.934	> 0.972
$t\bar{t}$	186.6 ± 0.4	44.5 ± 0.3	43.6 ± 0.3
$Z/\gamma^* \rightarrow \ell^+\ell^-$	N/A	7.4 ± 1.0	19.1 ± 1.3
$Z/\gamma^* \rightarrow \tau\tau$	11.2 ± 3.7	0.8 ± 0.3	0.35 ± 0.05
WW	5.6 ± 1.4	0.3 ± 0.1	0.13 ± 0.05
WZ	1.5 ± 0.5	0.28 ± 0.04	0.16 ± 0.01
ZZ	1.0 ± 0.5	0.34 ± 0.04	0.57 ± 0.04
Misidentified jets	15.9 ± 3.1	0.54 ± 0.48	3.7 ± 2.5
Total	221.7 ± 5.1	54.2 ± 1.2	67.7 ± 3.9
Observed	193	58	68

TEMPLATES

After the final event selection, $\cos\theta^*$ is calculated for each event by using the reconstructed top quark and W boson four-momenta. In the ℓ +jets decay channel, the four-momenta are reconstructed using a kinematic fit with the constraints: (i) two jets should give the invariant mass of the W boson ($80.4 \text{ GeV}/c^2$), (ii) the invariant mass of the lepton and neutrino should be the W boson mass, (iii) the mass of the reconstructed top and anti-top quark should be $172.5 \text{ GeV}/c^2$, and (iv) the \vec{p}_T of the $t\bar{t}$ system should be opposite that of the unclustered energy in the event. The four highest- p_T jets in each event are used in the fit, and among the twelve possible permutations in the assignment of the jets to initial partons, the solution with the highest probability is chosen, considering both the NN_b values of the four jets and χ^2_k . This procedure selects the correct jet assignment in 59% of MC $t\bar{t}$ events. With the jet assigned, the complete kinematics of the $t\bar{t}$ decay products (i.e., including the neutrino) are determined, allowing us to boost to the rest frames of each W boson in the event. We compute $\cos\theta^*$ for the W boson that decays leptonically. The hadronic W boson decay from the other top quark in the event also contains information about the helicity of that W boson, but since we do not distinguish between jets formed from up-type and down-type quarks, we can not identify the down-type fermion to calculate $\cos\theta^*$. We therefore calculate only $|\cos\theta^*|$, which is identical for both jets in the rest frame of the hadronically decaying W boson. Left-handed and right-handed W bosons have identical $|\cos\theta^*|$ distributions, but we can distinguish either of those states from longitudinal W bosons, thereby improving the precision of the measurement.

In the dilepton decay channel, the presence of two neutrinos prevents a constrained kinematic fit, but with the assumption that the top quark mass is $172.5 \text{ GeV}/c^2$, an algebraic solution for the neutrino momenta can be obtained (up to a two-fold ambiguity in pairing the jets and leptons, and a four-fold solution ambiguity). To account for the lepton and jet energy resolutions, the procedure described above is repeated 500 times with the energies fluctuated according to their uncertainties, and the average of all the solutions is used as the value of the $\cos\theta^*$ for

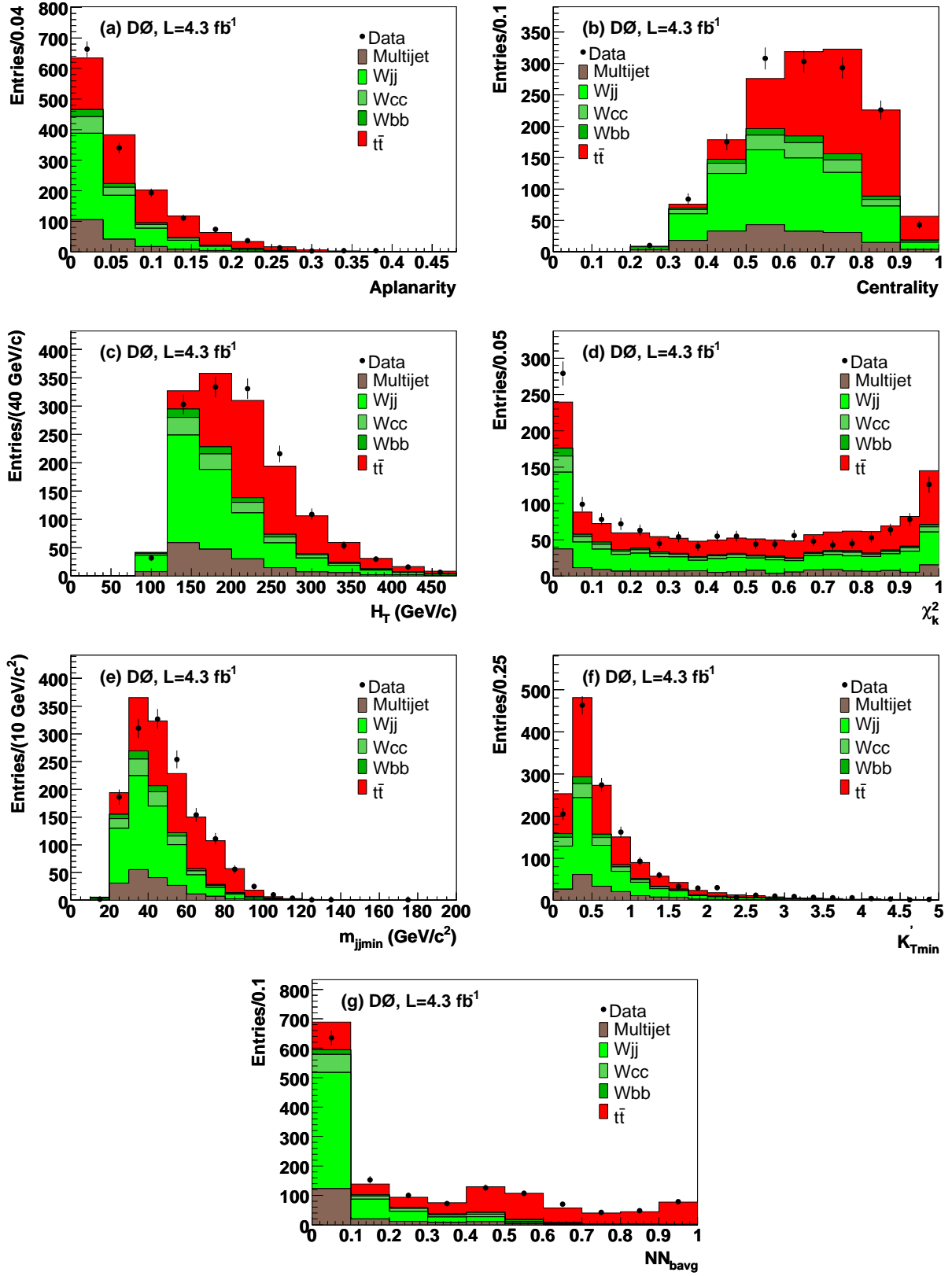


FIG. 1: (Color online) Comparison of data and MC of the variables for preselected events, chosen for the best likelihood discriminant L_t in the e +jets channel: (a) \mathcal{A} , (b) \mathcal{C} , (c) H_T , (d) χ_k^2 , (e) m_{jjmin} , (f) K_{Tmin} , and (g) NN_{bavg} . The uncertainties on the data points are statistical only.

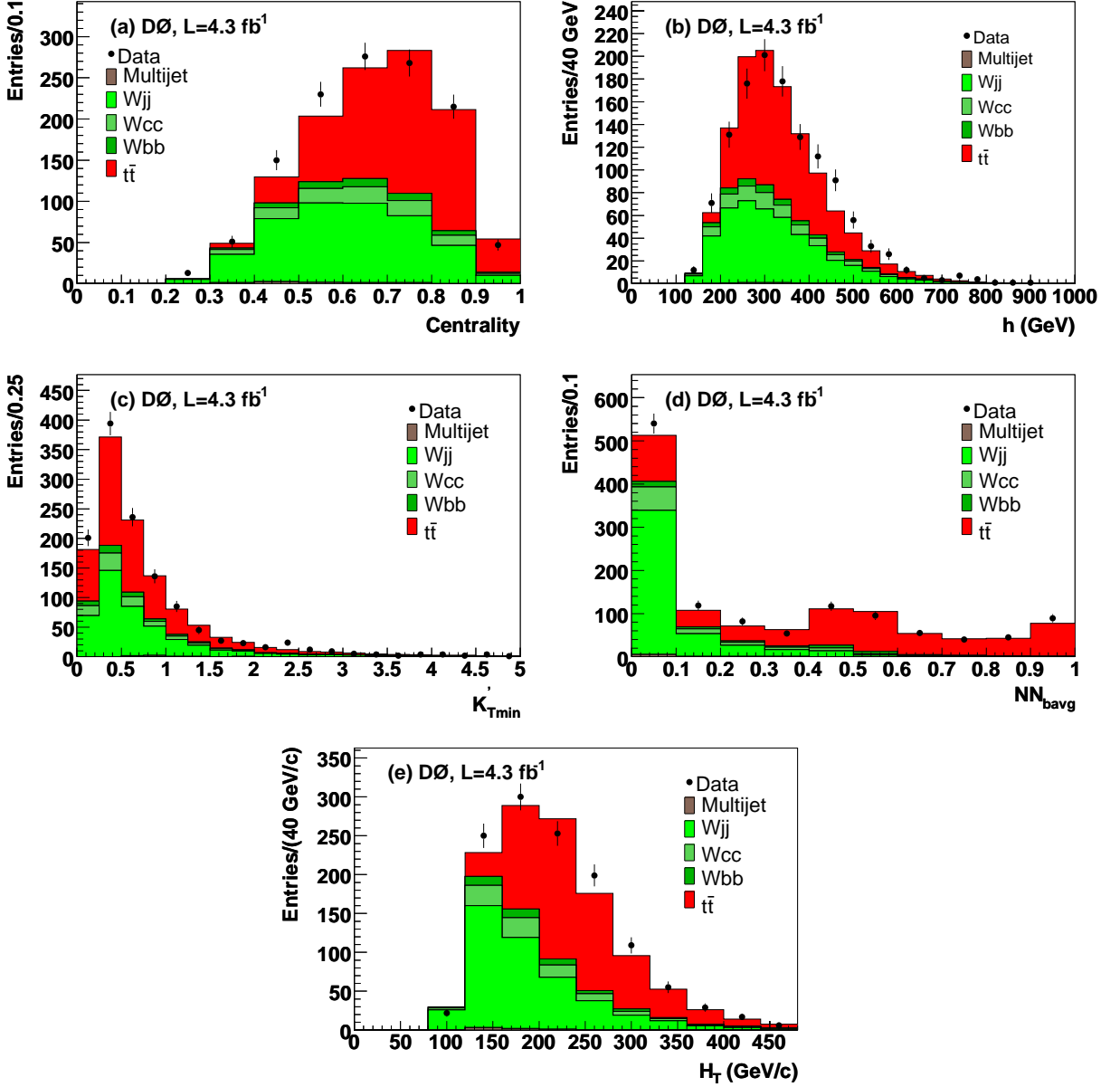


FIG. 2: (Color online) Comparison of data and MC of the variables for preselected events, chosen for the best likelihood discriminant L_t in the μ +jets channel: (a) C , (b) h , (c) K'_{Tmin} , (d) NN_{bavg} and (e) H_T . The uncertainties on the data points are statistical only.

each top quark.

As mentioned above, the extraction of both f_0 and f_+ requires comparing the data with the MC models in which both of these values are varied. Since ALPGEN can only produce linear combinations of $V - A$ and $V + A$ tWb couplings, it is unable to produce non-SM f_0 values, and can produce f_+ values only in the range $[0, 0.30]$. We therefore start with ALPGEN $V - A$ and $V + A$ samples, and divide the samples in bins of parton-level $\cos\theta^*$. For each bin, we note the efficiency for the event to satisfy the event selection and the distribution of reconstructed $\cos\theta^*$ values. With this information we determine the

expected distribution of reconstructed $\cos\theta^*$ values for any assumed W helicity fractions, and in particular we choose to derive the distributions expected for purely left-handed, longitudinal, or right-handed W boson, as shown in Fig. 8. The deficit of entries near $\cos\theta^* = -1$ relative to the expectation from Eq. 4 is due to the p_T requirement imposed when selecting leptons. We verify the reweighting procedure by comparing the generated $V \pm A$ ALPGEN samples with the combination of reweighted distributions expected for $V \pm A$ couplings, and find that these distributions agree within the MC statistics. The templates for background samples are obtained directly

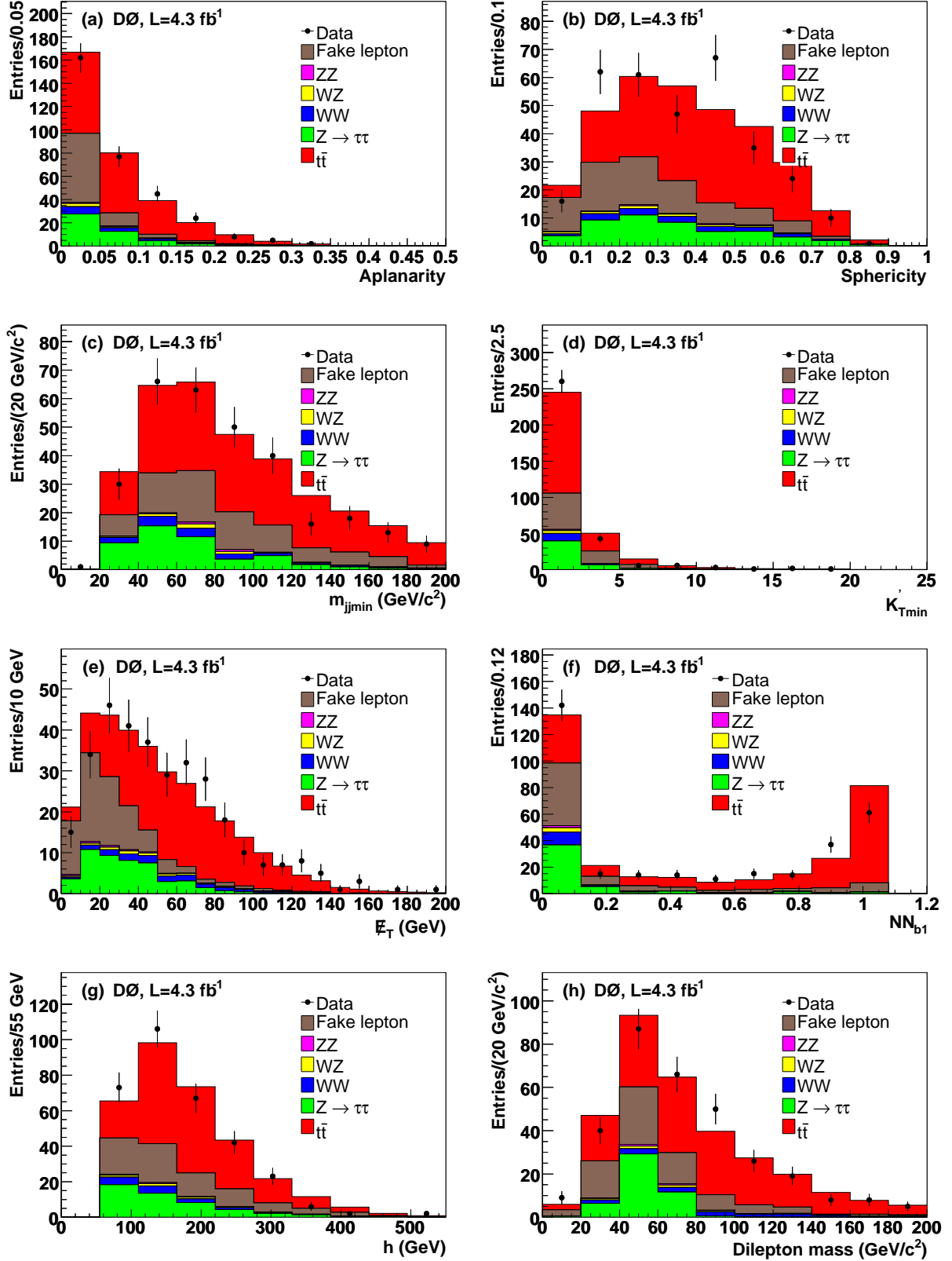


FIG. 3: (Color online) Comparison of data and MC of the variables for preselected events, chosen for the best likelihood discriminant L_t in the $e\mu$ channel: (a) \mathcal{A} , (b) \mathcal{S} , (c) m_{jjmin} , (d) K'_{Tmin} , (e) E_T , (f) NN_{b1} , (g) h , and (h) $m_{\ell\ell}$. The uncertainties on the data points are statistical only.

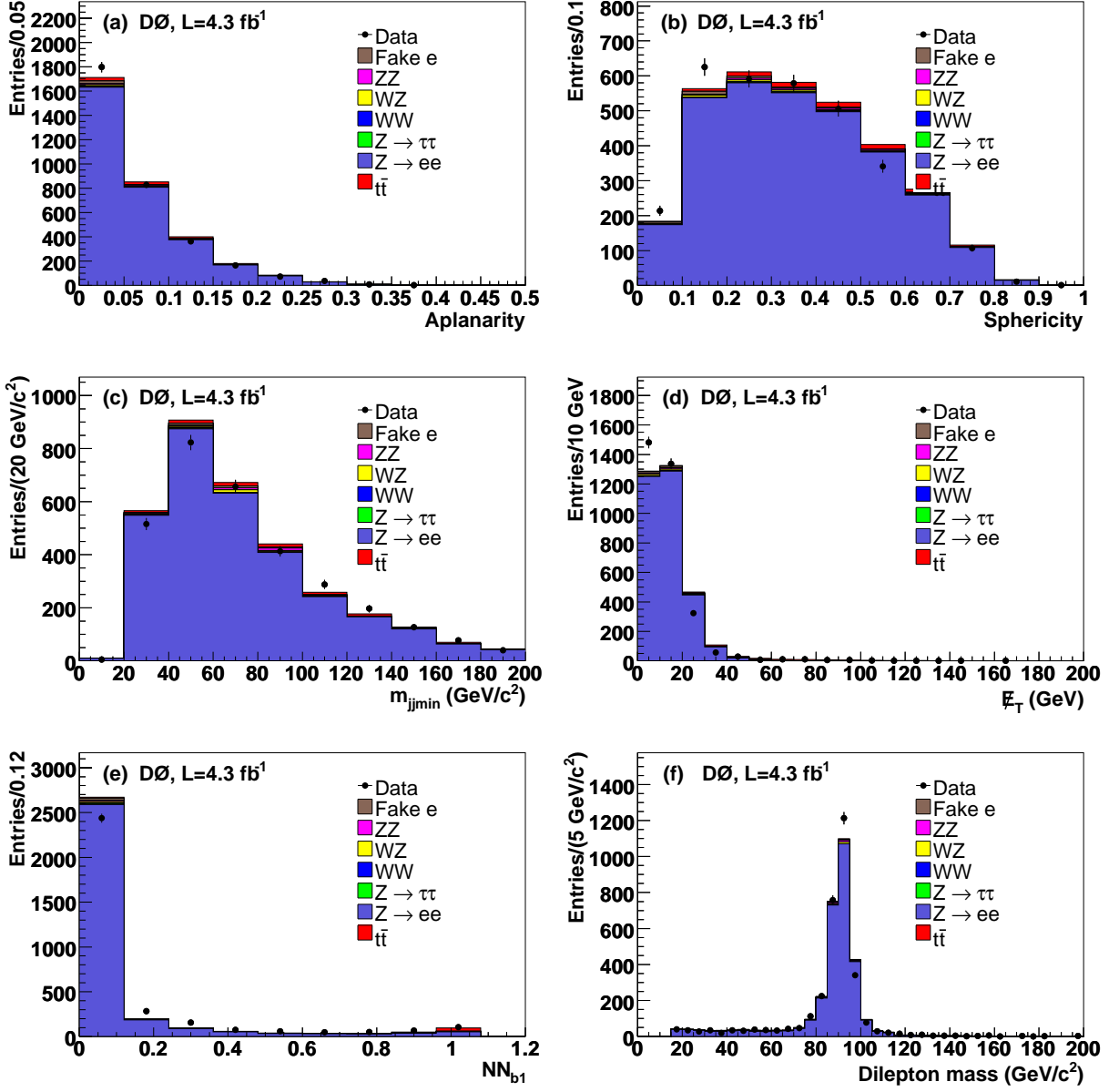


FIG. 4: (Color online) Comparison of data and MC of the variables for preselected events, chosen for the best likelihood discriminant L_t in the ee channel: (a) \mathcal{A} , (b) \mathcal{S} , (c) m_{jjmin} , (d) E_T , (e) NN_{b1} , and (f) $m_{\ell\ell}$. The uncertainties on the data points are statistical only.

from the relevant MC or data background samples, and are shown in Fig. 9.

MODEL-INDEPENDENT W HELICITY FIT

The W boson helicity fractions are extracted by computing a binned Poisson likelihood $L(f_0, f_+)$ with the distribution of $\cos\theta^*$ in the data to be consistent with the sum of signal and background templates. The likelihood is a function of the W boson helicity fractions f_0

and f_+ , defined as

$$L(f_0, f_+) = \prod_{i=1}^{N_{\text{chan}}} \prod_{j=1}^{N_{\text{bkg},i}} e^{-(n_{b,ij} - \bar{n}_{b,ij})^2 / 2\sigma_{b,ij}^2} \times \prod_{k=1}^{N_{\text{bins},i}} P(d_{ik}; n_{ik}) \quad (10)$$

where $P(d_{ik}; n_{ik})$ is the Poisson probability for observing d_{ik} events given a mean expectation value n_{ik} , N_{chan} is the number of channels in the fit (a maximum of five

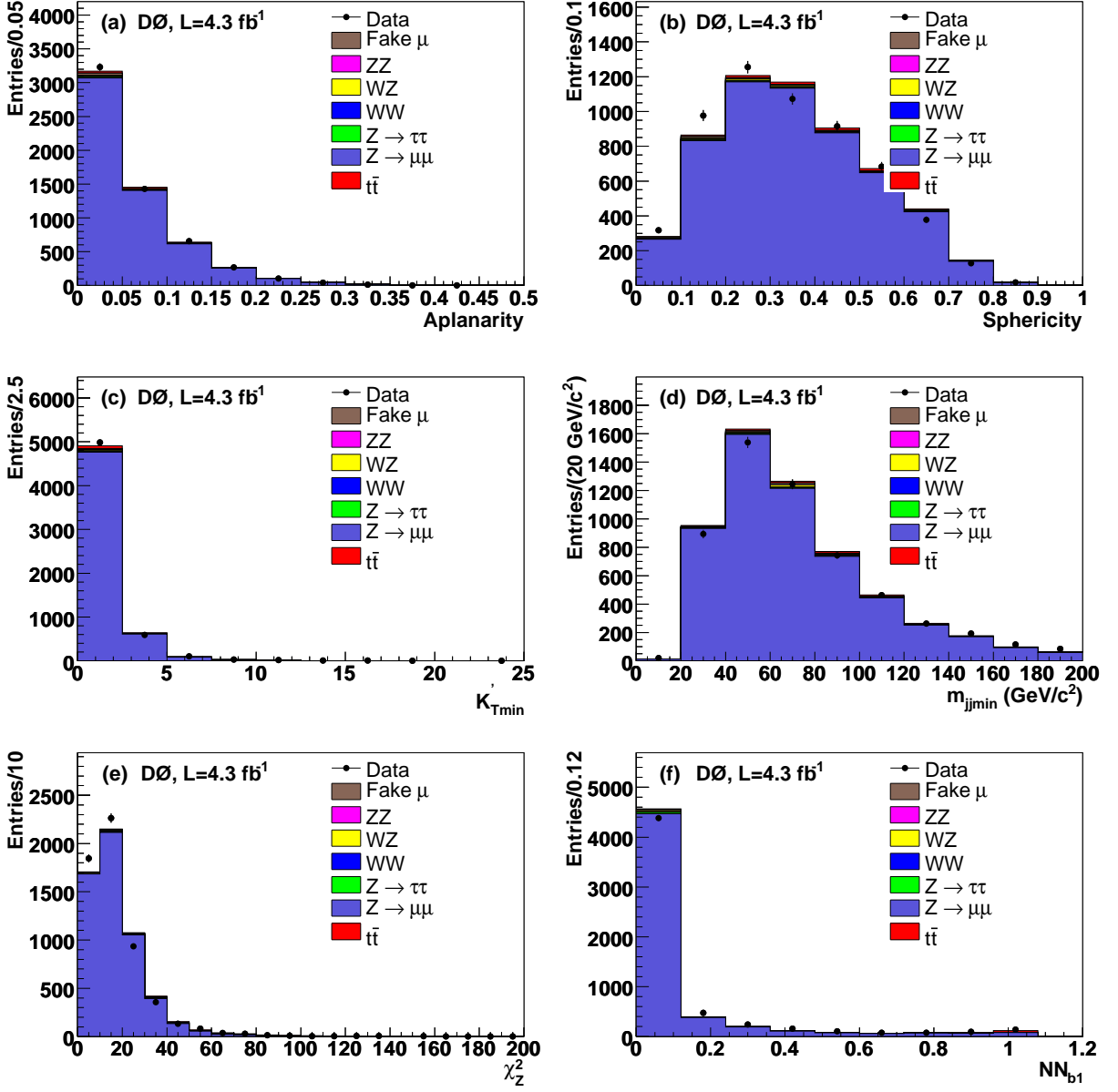


FIG. 5: (Color online) Comparison of data and MC of the variables for preselected events, chosen for the best likelihood discriminant L_t in the $\mu\mu$ channel: (a) \mathcal{A} , (b) \mathcal{S} , (c) $K'_{T\min}$, (d) $m_{jj\min}$, (e) χ^2_Z , and (f) NN_{b1} . The uncertainties on the data points are statistical only.

in this analysis: $e+\text{jets}$, $\mu+\text{jets}$, $e\mu$, ee , and $\mu\mu$), $N_{\text{bkg},i}$ is the number of background sources in the i^{th} channel, $N_{\text{bins},i}$ is the number of bins in the $\cos\theta^*$ distribution for any given channel (plus the number of bins in the $|\cos\theta^*|$ distribution for hadronic W boson decays in the $\ell+\text{jets}$ channels), $\bar{n}_{b,ij}$ is the nominal number of $\cos\theta^*$ measurements from the j^{th} background contributing to the i^{th} channel, $\sigma_{b,ij}$ is the uncertainty on $\bar{n}_{b,ij}$, $n_{b,ij}$ is the fitted number of events for this background, d_{ik} is the number of data events in the k^{th} bin of $\cos\theta^*$ for the i^{th} channel, and n_{ik} is the predicted sum of signal and

background events in that bin. The n_{ik} can be expressed as

$$n_{ik} = n_{s,i} \frac{\varepsilon_0 f_0 p_{0,ik} + \varepsilon_+ f_+ p_{+,ik} + \varepsilon_- (1 - f_0 - f_+) p_{-,ik}}{f_- \varepsilon_- + f_0 \varepsilon_0 + f_+ \varepsilon_+} + \sum_{j=1}^{N_{\text{bkg}}} n_{b,ij} p_{b,ijk} \quad (11)$$

where $n_{s,i}$ represents the number of $\cos\theta^*$ measurements from signal events in a given channel, the p represent the probabilities for an event from some source to appear in

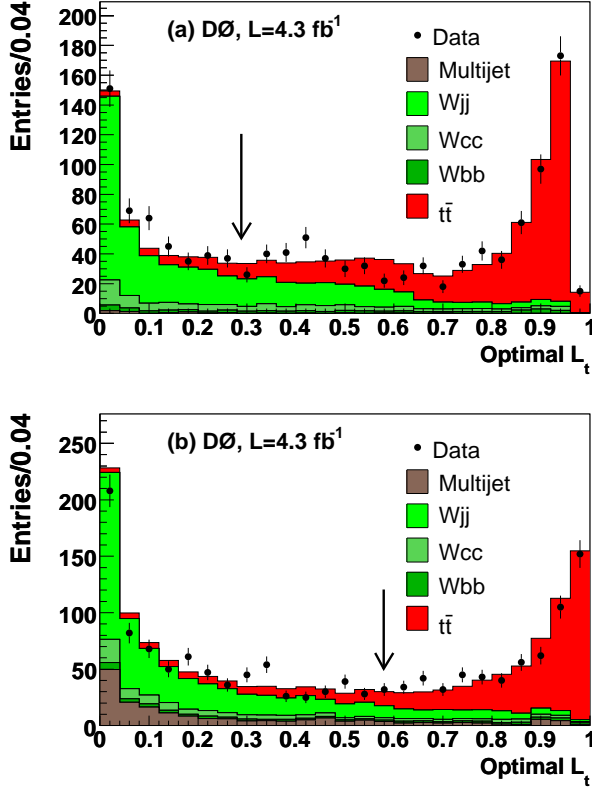


FIG. 6: (Color online) Best L_t variable for the (a) μ +jets and (b) e +jets channels. The normalization of the signal and background models is determined by the Poisson maximum likelihood fit to the L_t distribution. The arrows mark the required L_t values for events in each channel.

bin k for channel i (as determined from the templates), and the subscripts $0, +, -$ refer to the templates for $t\bar{t}$ events in which the W bosons have zero, negative, or positive helicity, and the subscript b, i refers to the templates for the i^{th} background source. The efficiency for a $t\bar{t}$ event to satisfy the selection criteria depends upon the helicity states of the two W bosons in the event; the ε are therefore necessary to translate the fractions of events with different helicity states in the selected sample to the fractions that were produced. The quantity ε_λ is defined as

$$\varepsilon_\lambda = \sum_{\lambda'} f_{\lambda'} \varepsilon_{\lambda\lambda'} \quad (12)$$

where $\varepsilon_{\lambda\lambda'}$ is the relative efficiency for events with W bosons in the λ and λ' helicity states to satisfy the selection criteria. The values of $\varepsilon_{\lambda\lambda'}$ for each $t\bar{t}$ decay channel are given in Table VI. While performing the fit, both f_0 and f_+ are allowed to float freely, and the measured W helicity fractions correspond to those leading to the highest likelihood value.

We check the performance of the fit using simulated ensembles of events, with all values of f_0 and f_+ from 0

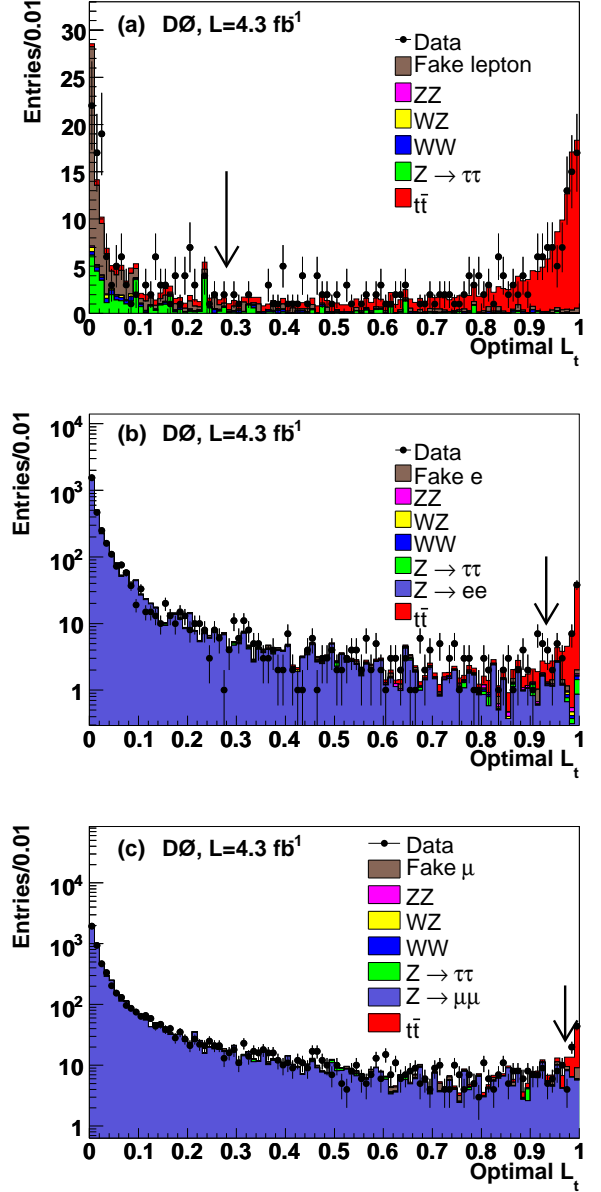


FIG. 7: (Color online) Best L_t variable for the (a) $e\mu$, (b) ee and (c) $\mu\mu$ decay channels. The normalization of the signal and background models is determined by the Poisson maximum likelihood fit to the L_t distribution. The arrows mark the required L_t values for events in each channel.

through 1 as inputs in increments of 0.1, with the sum of f_0 and f_+ not exceeding unity. We simulate input data distributions for the various values by combining the pure left-handed, longitudinal, and right-handed templates in the assumed proportions. In these ensembles, we draw a random subset of the simulated events, with the number of events chosen in each channel fixed to the number observed in data. Within the constant total number of events, the numbers of signal and background events are fluctuated binomially around the expected values. Each

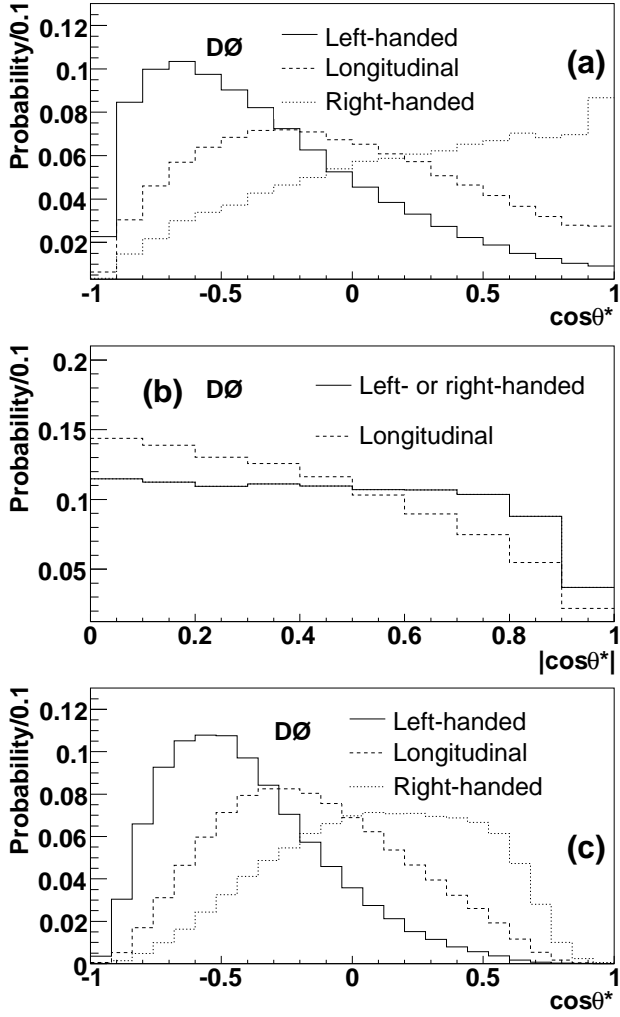


FIG. 8: Distribution of $\cos\theta^*$ in $t\bar{t}$ MC samples that were reweighted to derive the distributions for purely left-handed, longitudinal, or right-handed W bosons. The distribution for leptonically- and hadronically-decaying W bosons in ℓ +jets events are shown in (a) and (b), respectively, and the distribution for dilepton events is shown in (c). For hadronically decaying W bosons the $\cos\theta^*$ distribution for left- and right-handed W bosons are identical. All of the distributions are normalized to unity.

of these sets of simulated events is passed through the maximum likelihood fit using the standard $\cos\theta^*$ templates. We find that the average fit output value is close to the input value across the entire range of possible values for the helicity fractions, with the small differences between the input and output values being consistent with statistical fluctuations in the ensembles. As an example, the set of f_0 and f_+ values obtained when $t\bar{t}$ events are drawn in the proportions expected in the SM is shown in Fig. 10.

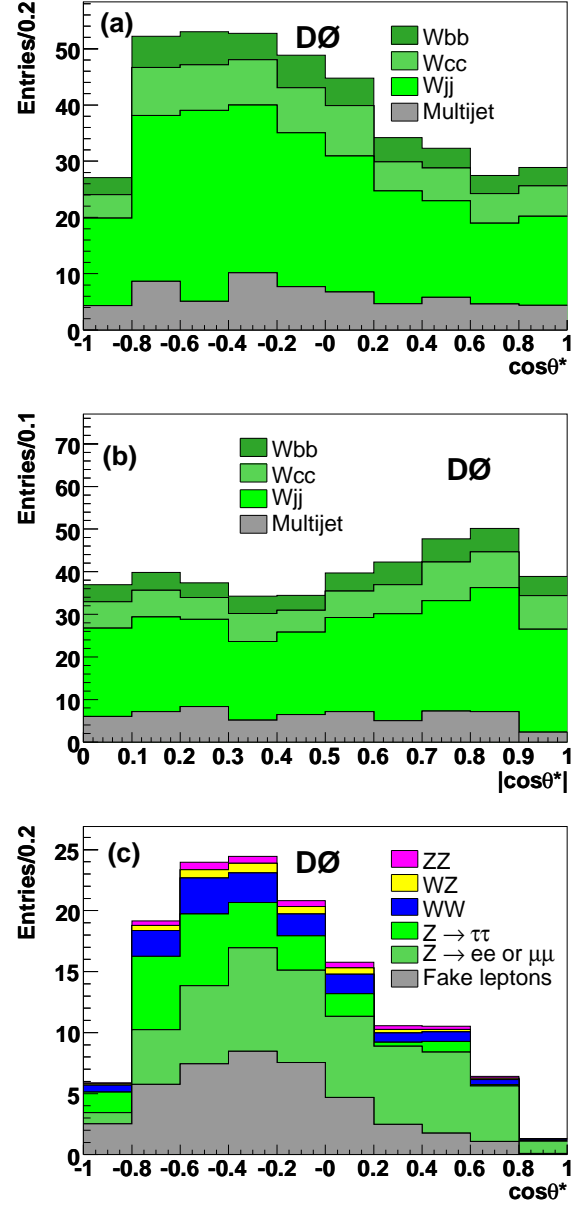


FIG. 9: (Color online) Distribution of $\cos\theta^*$ in background samples. The distribution for leptonically- and hadronically-decaying W bosons in ℓ +jets events are shown in (a) and (b), respectively, and the distribution for dilepton events is shown in (c). All of the distributions are normalized to the expected yield for each source of background.

SYSTEMATIC UNCERTAINTIES

Systematic uncertainties are evaluated using simulated event ensembles in which both changes in the background yield and changes in the shape of the $\cos\theta^*$ templates in signal and background are considered. The simulated samples from which the events are drawn can be either the nominal samples or samples in which the systematic effect under study has been shifted away from the nom-

TABLE VI: Efficiencies of different W boson helicity configurations in $t\bar{t}$ events to pass the selection criteria, relative to the efficiencies for a mixture of $V - A$ and $V + A$ events. The indices $-$, 0 and $+$ correspond to the helicity states of the two W bosons, and their order is leptonic W , hadronic W for the ℓ +jets channel, and arbitrary for dilepton channels (where there is no distinction between the two W bosons in the event). Small differences in values in the dilepton channels under interchange of the indices are from variations in MC statistics.

	e +jets	μ +jets	$e\mu$	ee	$\mu\mu$
ε_{--}	0.76	0.73	0.67	0.68	0.68
ε_{-0}	0.87	0.83	0.84	0.86	0.85
ε_{-+}	0.76	0.73	0.88	0.89	0.89
ε_{0-}	0.94	0.95	0.85	0.86	0.87
ε_{00}	1.08	1.09	1.06	1.05	1.05
ε_{0+}	0.94	0.95	1.10	1.05	1.05
ε_{+-}	0.92	0.96	0.89	0.88	0.91
ε_{+0}	1.06	1.11	1.12	1.03	1.07
ε_{++}	0.92	0.96	1.15	0.99	1.03

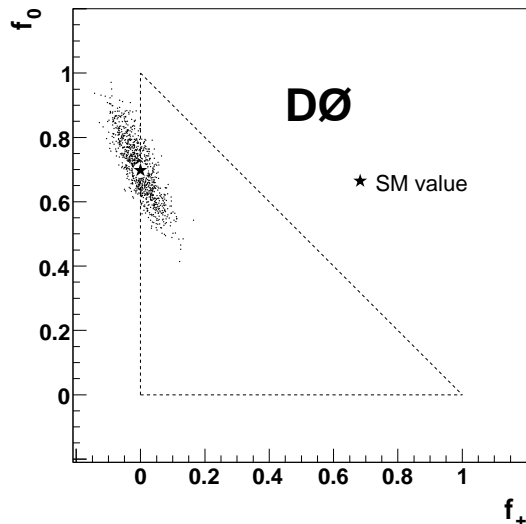


FIG. 10: Fit values for f_0 and f_+ obtained with 1000 MC simulations of the W boson helicity measurement. The SM helicity fractions, marked by the star, were taken as input to the simulations. The triangle corresponds to the physically allowed region where $f_0 + f_+ \leq 1$.

inal value. In general, the systematic uncertainties assigned to f_0 and f_+ are determined by taking an average of the absolute values of the differences in the average fit output values between the nominal and shifted $V - A$ and $V + A$ samples.

The jet energy scale, jet energy resolution, and jet identification efficiency each have relatively small uncertainties that are difficult to observe above fluctuations in the MC samples. To make the effects more visible, we vary these quantities by ± 5 standard deviations, and then di-

vide the resulting differences in the average fit output by 5. The top quark mass uncertainty corresponds to shifting m_t by $1.4 \text{ GeV}/c^2$, which is the sum in quadrature of the uncertainty on the world average m_t ($1.1 \text{ GeV}/c^2$) and the difference between the world average value ($173.3 \text{ GeV}/c^2$) and the value assumed in the analysis ($172.5 \text{ GeV}/c^2$). We evaluate the contribution of template statistics to the uncertainty by repeating the fit to the data 1000 times, fluctuating the signal and background distributions according to their statistics in each fit. The uncertainties due to the modeling of $t\bar{t}$ events are separated into several categories and evaluated using special-purpose MC samples. The uncertainty in the model of gluon radiation is assessed using PYTHIA MC samples in which the amount of gluon radiation is shifted upwards and downwards; the impact of NLO effects is assessed by comparing the default leading-order ALPGEN generator with the NLO generator MC@NLO [19]; the uncertainty in the hadronic showering model is assessed by comparing ALPGEN events showered with PYTHIA and with HERWIG [20]; and lastly, the impact of color reconnection effects is assessed by comparing PYTHIA samples where the underlying event model does and does not include color reconnection. The uncertainty due to data and MC differences in the background $\cos\theta^*$ distribution is derived by taking the ratio of the data and the MC distribution for a background-enriched sample (defined by requiring that events have low values of L_t) and then using that ratio to re-weight the distribution of background MC events that satisfy the standard selection. The uncertainty in the heavy flavor content of the background is estimated by varying the fraction of background events with heavy flavor jets by $\pm 20\%$. Uncertainties due to the fragmentation of b jets are evaluated by comparing the default fragmentation model, the Bowler scheme [21] tuned to data collected at the CERN LEP collider, with an alternate model tuned to data collected by the SLD collaboration [22]. Uncertainties in the parton distribution functions (PDFs) are estimated using the set of 2×20 errors provided for the CTEQ6M [23] PDF. The analysis consistency uncertainty reflects the typical difference between the input helicity fractions and the average output values observed in fits to simulated event ensembles. Finally, we include an uncertainty corresponding to muon triggers and identification, as control samples indicate some substantial data/MC discrepancies for the loose selection we use. All the systematic uncertainties are summarized in Table VII.

TABLE VII: Summary of the absolute systematic uncertainties on f_+ and f_0 .

Source	Uncertainty (f_+)	Uncertainty (f_0)
Jet energy scale	0.007	0.009
Jet energy resolution	0.004	0.009
Jet ID	0.004	0.004
Top quark mass	0.011	0.009
Template statistics	0.012	0.023
$t\bar{t}$ model	0.022	0.033
Background model	0.006	0.017
Heavy flavor fraction	0.011	0.026
b fragmentation	0.000	0.001
PDF	0.000	0.000
Analysis consistency	0.004	0.006
Muon ID	0.003	0.021
Muon trigger	0.004	0.020
Total	0.032	0.060

RESULT

Applying the model independent fit to the Run IIb data, we find

$$\begin{aligned} f_0 &= 0.739 \pm 0.091 \text{ (stat.)} \pm 0.060 \text{ (syst.)} \\ f_+ &= -0.002 \pm 0.045 \text{ (stat.)} \pm 0.032 \text{ (syst.)}. \end{aligned} \quad (13)$$

The comparison between the best-fit model and the data is shown in Fig. 11, and the 68% and 95% C.L. contours in the (f_+, f_0) plane are shown in Fig. 12(a). To account for systematic uncertainties, we perform a MC smearing of the L distribution, where the width of the smearing in f_0 and f_+ is given by the systematic uncertainty on each helicity fraction, and the correlation coefficient of -0.83 between them is taken into account.

To assess the consistency of the result with the SM, we note that the change in $-\ln L(f_0, f_+)$ (Eq. 10) between the best fit and the SM points is 0.24 considering only statistical uncertainties and 0.16 when systematic uncertainties are included. The probability of observing a greater deviation from the SM due to fluctuations in the data is 78% when only the statistical uncertainty is considered and 85% when both statistical and systematic uncertainties are considered.

We have also split the data sample in various ways to check the internal consistency of the measurement. Using ℓ +jets events only, we find

$$\begin{aligned} f_0 &= 0.767 \pm 0.117 \text{ (stat.)}, \\ f_+ &= 0.018 \pm 0.061 \text{ (stat.)}; \end{aligned} \quad (14)$$

and when using only dilepton events we find

$$\begin{aligned} f_0 &= 0.677 \pm 0.144 \text{ (stat.)}, \\ f_+ &= -0.013 \pm 0.065 \text{ (stat.)}. \end{aligned} \quad (15)$$

We also divide the sample into events with only electrons (e +jets and ee) and events with only muons

(μ +jets and $\mu\mu$). The results for electrons only are

$$\begin{aligned} f_0 &= 0.816 \pm 0.142 \text{ (stat.)}, \\ f_+ &= -0.063 \pm 0.066 \text{ (stat.)}, \end{aligned} \quad (16)$$

and for muons only are

$$\begin{aligned} f_0 &= 0.618 \pm 0.150 \text{ (stat.)}, \\ f_+ &= 0.130 \pm 0.081 \text{ (stat.)}. \end{aligned} \quad (17)$$

Finally, we perform fits in which one of the two helicity fractions is fixed to its SM value. Constraining f_0 , we find

$$f_+ = 0.014 \pm 0.025 \pm \text{(stat.)} \pm 0.028 \text{(syst.)}, \quad (18)$$

We also constrain f_+ and measure f_0 , finding

$$f_0 = 0.735 \pm 0.051 \text{ (stat.)} \pm 0.051 \text{(syst.)}. \quad (19)$$

COMBINATION WITH OUR PREVIOUS MEASUREMENT

To combine this result with the previous measurement from Ref. [6], we repeat the maximum likelihood fit with the earlier and current data samples and their respective MC models, treating them as separate channels in the fit. This is equivalent to multiplying the two-dimensional likelihood distributions in f_0 and f_+ corresponding to the two data sets. We determine the systematic uncertainty on the combined result by treating most uncertainties as correlated (the exception is template statistics) and propagating the uncertainties to the combined result. The results are presented in Table VIII.

TABLE VIII: Summary of the combined systematic uncertainties on f_+ and f_0 for Run IIa and Run IIb.

Source	Uncertainty (f_+)	Uncertainty (f_0)
Jet energy scale	0.009	0.010
Jet energy resolution	0.004	0.008
Jet ID	0.005	0.007
Top mass	0.012	0.009
Template statistics	0.011	0.021
$t\bar{t}$ model	0.024	0.039
Background model	0.008	0.023
Heavy flavor fraction	0.010	0.022
b fragmentation	0.002	0.004
PDF	0.000	0.001
Analysis consistency	0.004	0.006
Muon ID	0.002	0.017
Muon trigger	0.003	0.024
Total	0.034	0.065

The combined result for the entire 5.4 fb^{-1} sample is

$$\begin{aligned} f_0 &= 0.669 \pm 0.078 \text{ (stat.)} \pm 0.065 \text{ (syst.)}, \\ f_+ &= 0.023 \pm 0.041 \text{ (stat.)} \pm 0.034 \text{ (syst.)}. \end{aligned} \quad (20)$$

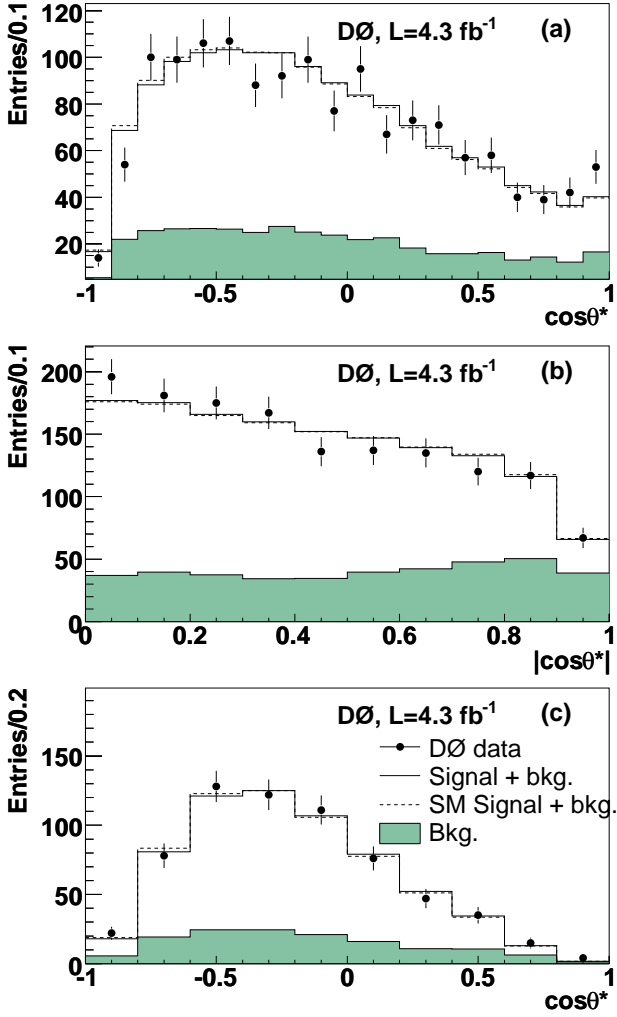


FIG. 11: (Color online) Comparison of the $\cos\theta^*$ distribution in Run IIb data and the global best-fit model (solid line) and the SM (dashed line) for (a) leptonic W boson decays in ℓ +jets events, (b) hadronic W boson decays in ℓ +jets events, and (c) dilepton events.

The combined likelihood distribution is presented in Figs. 12(b). The probability of observing a greater deviation from the SM due to fluctuations in the data is 83% when only statistical uncertainties are considered and 98% when systematic uncertainties are included.

Constraining f_0 to the SM value, we find

$$f_+ = 0.010 \pm 0.022 \text{ (stat.)} \pm 0.030 \text{ (syst.)} \quad (21)$$

and constraining f_+ to the SM value gives

$$f_0 = 0.708 \pm 0.044 \text{ (stat.)} \pm 0.048 \text{ (syst.)} \quad (22)$$

CONCLUSION

We have measured the helicity of W bosons arising from top quark decay in $t\bar{t}$ events using both the ℓ +jets

and dilepton decay channels and find

$$\begin{aligned} f_0 &= 0.669 \pm 0.102 & (23) \\ &[\pm 0.078 \text{ (stat.)} \pm 0.065 \text{ (syst.)}], \\ f_+ &= 0.023 \pm 0.053 \\ &[\pm 0.041 \text{ (stat.)} \pm 0.034 \text{ (syst.)}]. \end{aligned}$$

in a model-independent fit. The consistency of this measurement with the SM values $f_0 = 0.698$, $f_+ = 3.6 \times 10^{-4}$ is 98%. Therefore, we report no evidence for new physics at the tWb decay vertex.

ACKNOWLEDGEMENT

We thank the staffs at Fermilab and collaborating institutions, and acknowledge support from the DOE and NSF (USA); CEA and CNRS/IN2P3 (France); FASI, Rosatom and RFBR (Russia); CNPq, FAPERJ, FAPESP and FUNDUNESP (Brazil); DAE and DST (India); Colciencias (Colombia); CONACyT (Mexico); KRF and KOSEF (Korea); CONICET and UBACyT (Argentina); FOM (The Netherlands); STFC and the Royal Society (United Kingdom); MSMT and GACR (Czech Republic); CRC Program and NSERC (Canada); BMBF and DFG (Germany); SFI (Ireland); The Swedish Research Council (Sweden); and CAS and CNSF (China).

-
- [1] F. Abe *et al.* (CDF Collaboration), Phys. Rev. Lett. **74**, 2626 (1995).
 - [2] S. Abachi *et al.* (D0 Collaboration), Phys. Rev. Lett. **74**, 2632 (1995).
 - [3] M. Fischer *et al.*, Phys. Rev. D **63**, 031501(R) (2001).
 - [4] Tevatron Electroweak Working Group, arXiv:1007.3178[hep-ex] (2010).
 - [5] K. Nakamura *et al.* (Particle Data Group), J. Phys. G **37**, 075021 (2010).
 - [6] V.M. Abazov *et al.* (D0 Collaboration), Phys. Rev. Lett. **100**, 062004 (2008).
 - [7] T. Aaltonen *et al.* (CDF Collaboration), Phys. Rev. Lett. **105**, 042002 (2010).
 - [8] V.M. Abazov *et al.* (D0 Collaboration), Nucl. Instrum. Methods in Phys. Res. A **565**, 463 (2006).
 - [9] R. Angstadt *et al.*, Nucl. Instrum. Methods in Phys. Res. A **622**, 298 (2010).
 - [10] M. Abolins *et al.*, Nucl. Instrum. Methods in Phys. Res. A **584**, 75 (2008).
 - [11] M.L. Mangano, J. High Energy Phys. **07**, 001 (2003).
 - [12] T. Sjöstrand *et al.*, Computer Phys. Commun. **135** 238, (2001).
 - [13] S. Agostinelli *et al.*, Nucl. Instrum. Methods in Phys. Res. A **506**, 250 (2003).
 - [14] G.C. Blazey *et al.*, arXiv:hep-ex/0005012 (2000).
 - [15] V.M. Abazov *et al.* (D0 Collaboration), Nucl. Instrum. Methods in Phys. Res. A **620**, 490 (2010).
 - [16] V.M. Abazov *et al.* (D0 Collaboration), Phys. Lett. B **626**, 45 (2005).

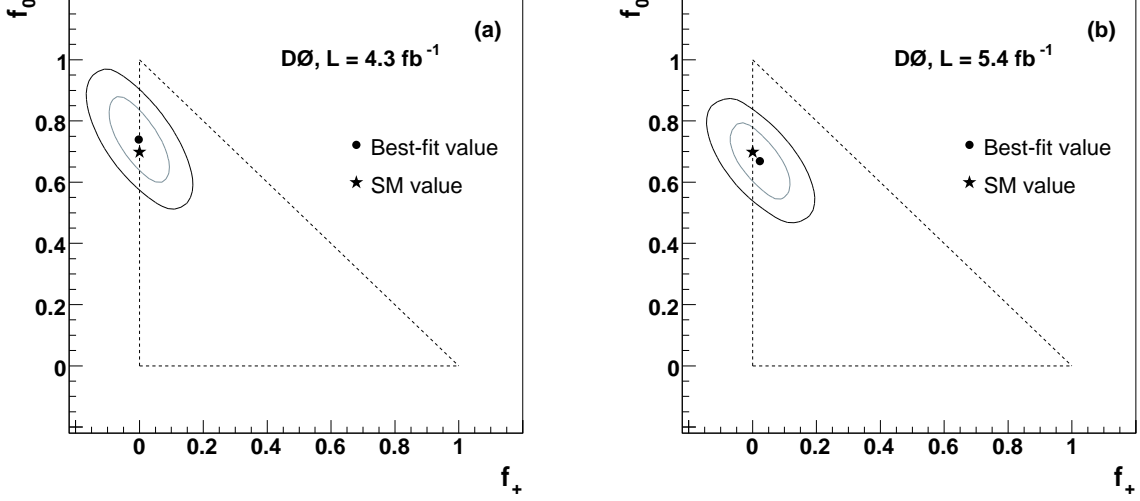


FIG. 12: Result of the model-independent W boson helicity fit for (a) the Run IIb data sample and (b) the combined Run IIa and Run IIb data sample. In both plots, the ellipses indicate the 68% and 95% C.L. contours, the dot shows the best-fit value, the triangle corresponds to the physically allowed region where $f_0 + f_+ \leq 1$, and the star marks the expectation from the SM.

- [17] F. Abe *et al.* (CDF Collaboration), Phys. Rev. D **50**, 2966 (1994).
- [18] S. Abachi *et al.* (D0 Collaboration), Phys. Rev. Lett. **74**, 2422 (1995).
- [19] S. Frixione and B. Webber, J. High Energy Phys. **06**, 29 (2002).
- [20] G. Corcella *et al.*, J. High Energy Phys. **01**, 010 (2001).
- [21] M.G. Bowler, Z. Phys. C **11** 169 (1981).
- [22] Y. Peters *et al.*, FERMILAB-TM-2425-E (2006).
- [23] J. Pumplin *et al.*, J. High Energy Phys. **07**, 012 (2002).